Int J Clin Exp Med 2015;8(4):4940-4953
www.ijcem.com /ISSN:1940-5901/IJCEM0005212

Original Article

Local delivery of rhVEGF$_{165}$ through biocoated nHA/coral block grafts in critical-sized dog mandible defects: a histological study at the early stages of bone healing

Bing Du[1], Yao Gao[2], Yue Deng[3], Yadong Zhao[4], Chunhua Lai[2], Zehong Guo[2], Mingdeng Rong[2], Lei Zhou[2]

[1]Center of Stomatology, The First People's Hospital of Foshan, Foshan, Guangdong, China; [2]Department of Oral Implantology, Guangdong Provincial Stomatological Hospital, Southern Medical University, Guangzhou 510280, China; [3]Department of Oral and Maxillofacial Surgery, Qingdao Stomatological Hospital, Qingdao 266003, China; [4]Department of Stomatology, Inner Mongolia People's Hospital, Hohhot, Inner Mongolia 010017, China

Received December 25, 2014; Accepted February 20, 2015; Epub April 15, 2015; Published April 30, 2015

Abstract: Alveolar defects of a critical size cannot heal completely without grafting. Thus, they represent a major clinical challenge to reconstructive surgery. Numerous types of grafts have been used to improve bone regeneration. In the case of particle grafts, the capacity for volume rebuilding and space maintaining is still not ideal, particularly for critical-sized bone defects. Although porous block grafts can overcome the above problems of particle grafts, they are still not widely used for critical-sized alveolar defects, because of their reduced efficacy in blood vessel and bone formation. Thus, in the present study, nano-hydroxyapatite/coralline (nHA/coral) blocks were pre-vascularized by coating them with vascular endothelial growth factor (VEGF), and then implanted in dogs with critical-sized mandibular defects. This model has possible applications in orthopedic and implant surgery. In vivo results indicate that the nHA/coral blocks allow cell and collagen ingrowth because of their suitable pore size and interconnectivity of pores. In addition, pre-vascularization properties were obtained by coating the scaffolds with VEGF. Histological and immunohistochemical examinations, as well as fluorescence analysis, revealed that the local delivery of VEGF can significantly improve neovascularization and mineralization of newly formed bone at the early stages of bone healing in this dog implantation model. Our data collectively show that nHA/coral blocks have possible applications in bone tissue engineering, and excellent results can be achieved by pre-vascularization with VEGF.

Keywords: Angiogenesis, bone regeneration, histology, tissue engineering

Introduction

Large alveolar defects can easily occur as a result of injury, tumors, or surgery [1, 2]. Despite the good ability of the alveolar bone to regenerate, once the defect reaches a critical size, the process of bone healing always fails or is delayed [3, 4]. Therefore, bone grafting is necessary for the restoration of critical-sized defects.

Currently, an autogenous graft is considered to be the gold standard for bone regeneration [5, 6], but this requires additional surgery. Consequently, this can lead to further injury and other complications; therefore, autogenous grafts cannot be widely applied to large defects. For coralline hydroxyapatite (CHA) particle grafts, cells and bone matrix can envelop CHA particles, and new bone growth can be evenly distributed in the space between the particles [7]. Owing to the excellent bone regeneration properties of CHA particles, it has been widely used in periodontal and implant surgery [8, 9]. The biggest disadvantage of CHA particle grafts is its poor ability to maintain space; as a result, predictable results for bone volume and remodeling cannot always be achieved [10]. Compared with autogenous block grafting, CHA block grafting is commercially available and free from size constraints. It can even be fabricated into certain shapes to remodel the shape of the defect. Moreover, compared with CHA particles, CHA blocks have improved space maintaining and bone volume rebuilding properties. However, the limitation of these scaf-

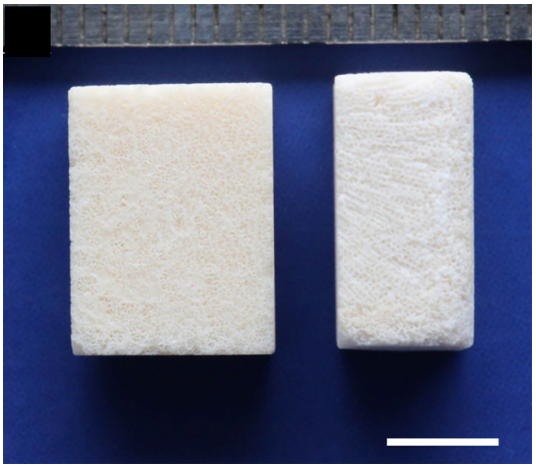

Figure 1. An image of the porous structure of the nHA/coral blocks with dimensions of 6 × 9 × 12 mm, white scale: 5 mm.

folds is the non-uniform blood supply within the block, especially in large-scale defects. Few studies about CHA block grafting in critical-size alveolar defects have been performed, and their clinical application was limited.

Bone healing is a complicated in vivo process; it involves the presence of a clot containing large numbers of mesenchymal cells, then a proliferation and high metabolic level of osteoblasts and macrophages, followed by the regeneration of blood vessels and woven bone. The recruitment of progenitor cells to the injury site, neovascularization near the injury site, and angiogenesis are crucial at the early stages of bone repair [11-14]. However, even if optimal scaffolds are applied, critical-sized alveolar defects with poor vascularization around the block grafting site can also have poor bone healing because of ischemia. Therefore, it is necessary to improve the clinical success and application of block grafting by applying a pre-vascularization process before implantation [14, 15].

Angiogenesis is directed by a variety of growth factors in a complicated multi-step process, in which vascular endothelial growth factor (VEGF) has been identified as a potent angiogenic regulator [16]. A previous study has shown that VEGF can activate endothelial cells by stimulating their migration, proliferation, and the formation of vascular channels [17]. Moreover, it may act as a survival factor for endothelial cells and immature vessels. Furthermore, VEGF may recruit osteoclasts, monocytes, osteoblasts, and mesenchymal progenitor cells, and support their differentiation function and survival [18, 19]. Thus, the pre-vascularization of scaffolds by coating them with angiogenic growth factors may be one of the most feasible approaches for bone reconstruction andangiogenesis promotion in critical-sized alveolar defects. We hypothesized that: (1) porous nano-hydroxyapatite/coralline (nHA/coral) blocks can be an optimal grafting material in critical-sized mandible defects, with good bone regeneration performance; and (2) local delivery of rhVEGF$_{165}$ with the nHA/coral block used as a carrier can promote angiogenesis and osteogenesis at the early stages of bone healing.

Materials and methods

Scaffold characterization

The nano-hydroxyapatite/coral blocks used in this study had dimensions of 6 × 9 × 12 mm and were sterilized with γ-irradiation before use (**Figure 1**, supplied by Beijing YHJ Science and Trade Co. Ltd). The morphology, pore size, walls of the porous structure, and diameter of nHA crystals on the surface were analyzed with scanning electron microscopy (SEM, Jeol JSM-6300, operated at 20 kV).

Animals

The two beagle dogs (12-13 months old, mean weight 12.2 ± 0.3 kg) used in this study were provided by the Guangdong Provincial Medical Experimental Animal Center (license number: SYXK (yue) 2012-0081). Both exhibited fully erupted, healthy, permanent dentition. During the experiment, the animals were fed once per day with a soft-food diet and water. Experiments started after an adaptation period of 7 days. The animal experimental protocol was approved by the ethical committee of the Guangdong Provincial Stomatological Hospital.

Experimental design

The study was performed in two surgical phases. In the first phase, the extraction of the mandibular second, third, and fourth premolars, as well as the first and second molars (P2-M2), was performed bilaterally on each dog. Following tooth removal, four standardized box-

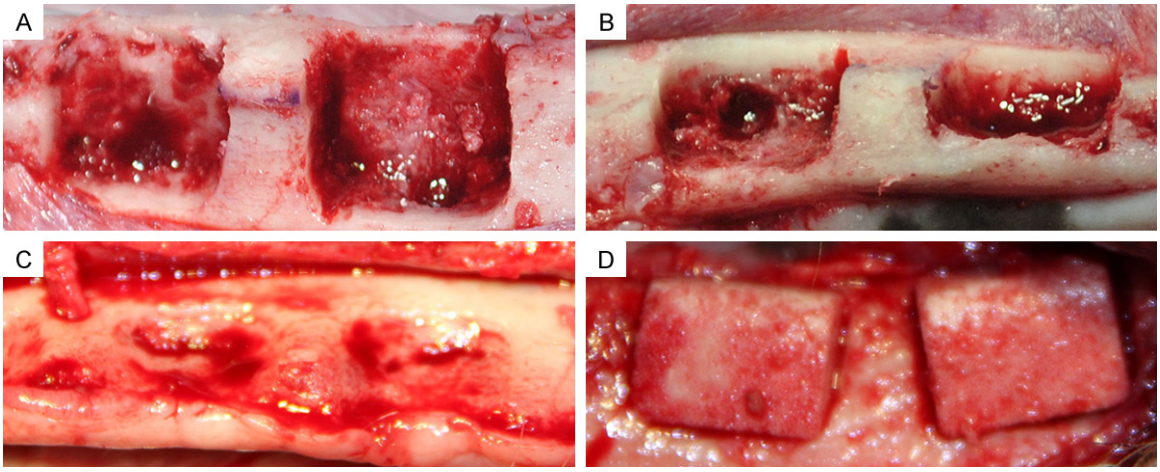

Figure 2. A and B. (Buccal view and occlusal view, respectively) Standardized box-type defects (9 mm in height from the crestal bone, 6 mm in depth from the surface of the buccal bone, and 12 mm in width mesiodistally; distance between defects is 4 mm) were surgically created at the buccal aspect of the alveolar ridge after removing teeth from the mandible. C. A chronic-type defect was achieved after eight weeks of submerged healing (occlusal view). D. After defect reshaping, nHA/coral blocks were implanted into defect sites (buccal view).

shaped defects were created through surgery at the buccal aspect of the alveolar ridge in the mandible (total number of defects created (n) = 8). After eight weeks of submerged healing, the chronic defects were reshaped and divided into nHA/coral and VEGF/nHA/coral sites in a split-mouth design. Uncoated nHA/coral blocks served as controls. All animals were euthanized after a submerged healing period of three weeks.

Surgical phase 1: tooth extraction and defect creation

Following intramuscular sedation with Sumian Xin (composition: 2,4-dimethylaniline thiazole, ethylenediaminetetraacetic acid, dihydroetorphine hydrochloride, and haloperidol; Animal Husbandry Research Institute, Jilin, China; 0.2 ml/kg body weight), anesthesia was performed by intravenously injecting 3% pentobarbital solution (Foshan Chemical Engineering Experimental Factory, Foshan, China; 0.3 ml/kg body weight). Before the surgery, Primacaine (Merignac Cedex, France; 0.2 ml/kg body weight) was injected locally into the surgical area of the mandible. In addition, intramuscular administration of benzylpenicillin (Longteng Pharmaceutical Company, Sichuan, China; 80 million U/d) was performed intra- and postoperatively for each animal for 7 days.

In the first surgery, mucoperiosteal flaps were reflected, and then the P2-M2 teeth were carefully removed bilaterally from the mandible of each dog. After tooth extraction, four standardized box-type defects (9 mm in height from the crestal bone, 6 mm in depth from the surface of the buccal bone, and 12 mm in width mesiodistally) were created in the buccal side of mandubule with carbide burs, as previously reported [20]. The lingual bone plates were left intact (**Figure 2A**, **2B**). All osteotomy procedures were performed with the flushing of sterile 0.9% physiological saline. The wounds were closed by means of interrupted sutures (Foosin Medical Supplies Inc, Weihai, China), and all surgical sites were allowed to heal for eight weeks.

Biocoating

To coat the nHA/coral blocks with VEGF, the lyophilized growth factors rhVEGF$_{165}$ (PeproTech, America) were dissolved in sterile PBS buffer under aseptic conditions and then injected into the blocks [21]. Each block was moistened with 0.25 ml of a 12 μg/ml rhVEGF$_{165}$ solution (3 μg of rhVEGF$_{165}$ per block) [22]. The control samples were soaked with 0.25 ml of sterile PBS buffer.

Surgical phase 2: defect reshaping and block grafting

In the second surgery, vestibular incisions were made and the full-thickness flaps were reflected to expose the block grafting sites in the

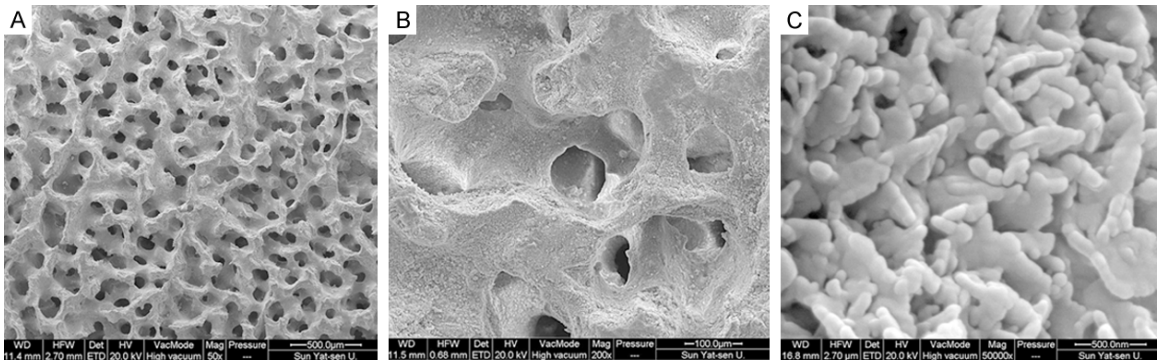

Figure 3. SEM images of a nHA/coral block: A. Nanoscale hydroxyapatite crystals were evenly distributed across the surface. B and C. All pores were sufficiently interconnected and distributed.

mandible (**Figure 2C**). Before implantation, the chronic defects were reshaped with carbide burs, and then the nHA/coral and rhVEGF$_{165}$-coated nHA/coral blocks were implanted in a split-mouth design (**Figure 2D**).

After periosteal-releasing incisions, the full-thickness flaps were advanced, coronally repositioned, and closed with interrupted sutures to ensure submerged healing for three weeks. Fluorochrome bone labels were given subcutaneously (10 mg/mL). Tetracycline (30 mg/kg body weight) and 10 mg/mL calcein (10 mg/kg body weight) were administered 13 and 14 days and 3 and 4 days before euthanizing the animals, respectively.

Histological observation and histomorphometrical analysis

After 3 weeks, the animals were euthanized with an overdose of anesthetics. The lower jaws were separated and soaked for a week in 4% neutral buffered formalin solution. The samples were then prepared with a carborundum disk, with each specimen composed of an implant and the surrounding bone tissue. Each sample was buccolingually cut in half; one half was embedded in resin and the other was embedded in paraffin.

Before embedding the samples in paraffin, they were decalcified in 10% EDTA and dehydrated using ascending grades of alcohol. After being embedded in paraffin, all samples were sectioned into three 5-mm-thick slices and stained with hematoxylin and eosin (HE) or Masson's trichrome. The three sections were evaluated separately by two blind observers using a digital microscope (BX51, Olympus Co., Tokyo, Japan) and digital camera (DP71, Olympus) at 10 × magnification (**Figure 4**). The whole scaffold and newly formed bone within the implants were then outlined and measured with the image analysis software Image-Pro Plus (Media Cybernetics, USA), and the percentage of new bone growth (PBF = newly formed bone area/total scaffold area) was measured (**Figure 4C**). Sections stained with Masson's trichrome were used to define the collagen secretion during the bone formation process as an indirect indicator of the quantity of newly formed bone.

Immunohistological staining

For immunohistochemical analysis, 5-μm-thick sections from independent samples were immunostained for von Willebrand factor (vWF), which is a protein present in large quantities in subendothelial matrices, such as blood vessel basement membranes [23]. All processes were performed following the manufacturer's protocol, using a rabbit anti-dog vWF primary antibody (1:1500) and biotinylated anti-rabbit IgG from a commercial kit (Dako, Germany). Then the sections were counterstained with hematoxylin. All sections were imaged with an Olympus BX51 light microscope and Olympus DP71 digital camera. Positive vWF staining of the blood vessels was counted manually at 20 × magnification within the scaffold area, and the neovascular density was calculated by Image Pro Plus Software, as previously reported [22].

Fluorescence analysis

Before embedding the samples in resin, they were dehydrated with a graded series of alcohol. Once embedded in the acrylic material,

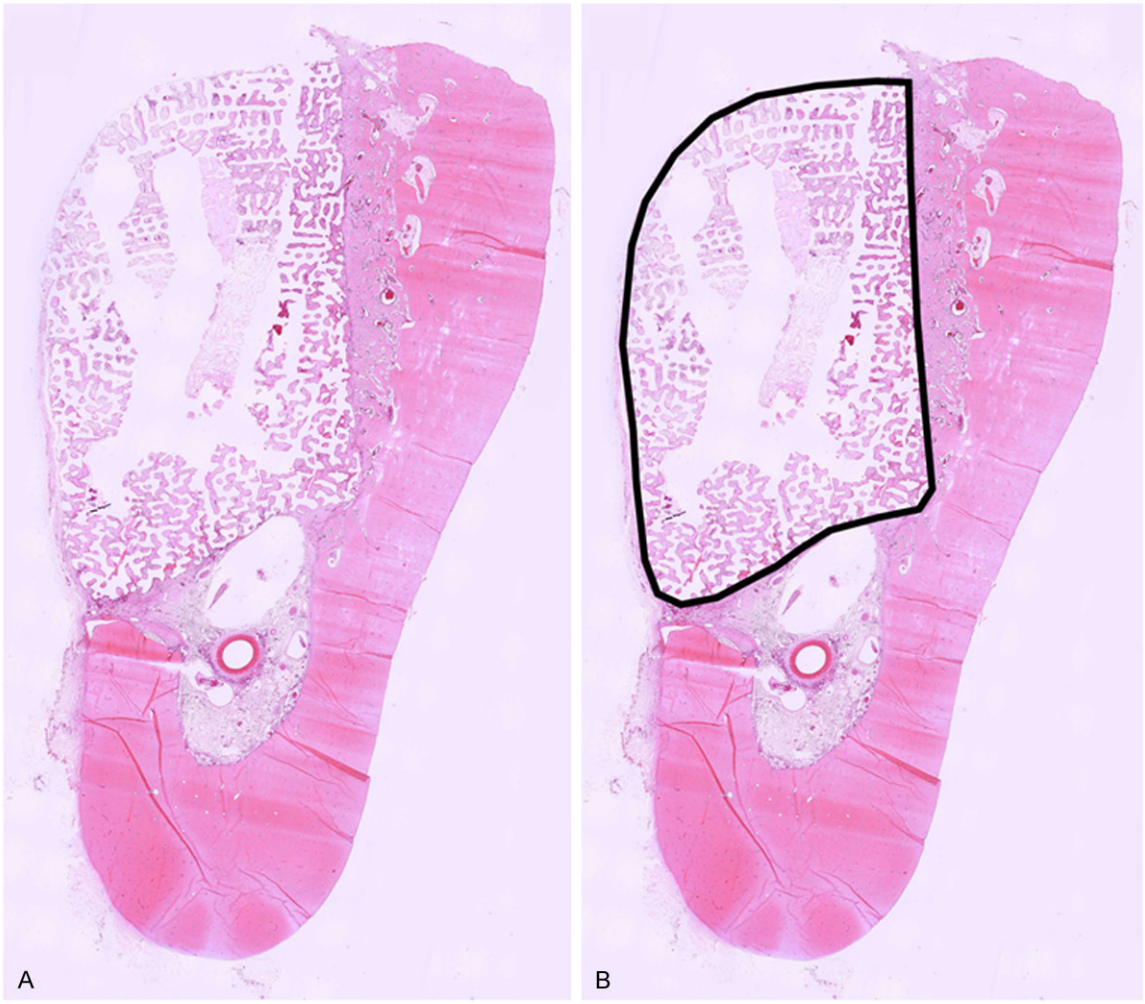
A
B

C

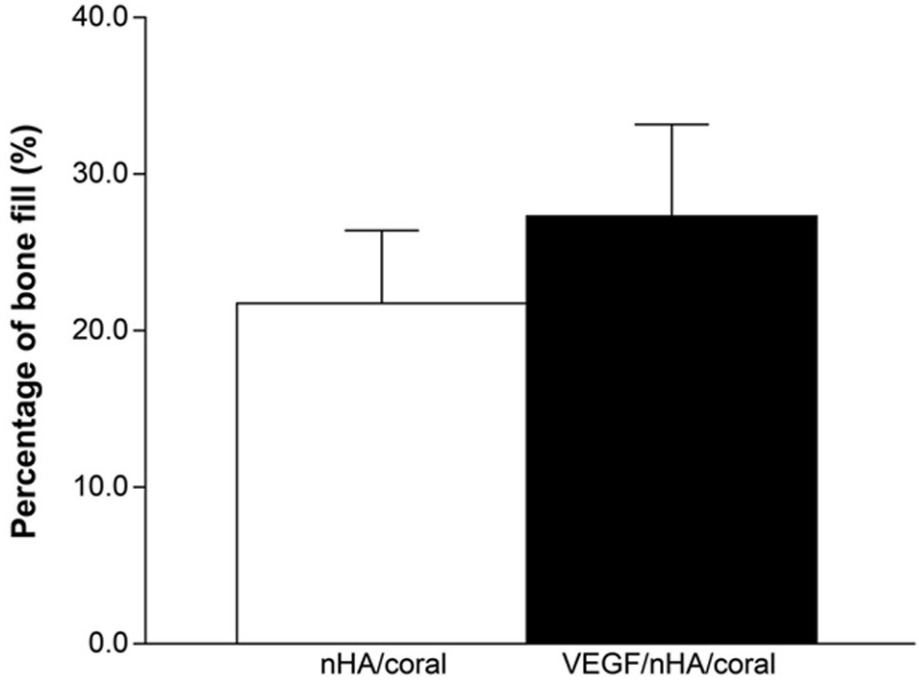
Percentage of bone fill (%)
40.0
30.0
20.0
10.0
0.0
nHA/coral
VEGF/nHA/coral

Figure 4. A. Decalcified sections grafted with two scaffolds. After 3 weeks, each defect was removed with the surrounding tissue, buccolingually sectioned, and stained with hematoxylin and eosin. B. The whole scaffold area (black line), which was identified by the Image-Pro Plus software. The percentage of new bone fill (PBF) was determined based on the size of the whole scaffold area. C. Histomorphometrical analysis of newly formed bone calculated from HE staining. The local delivery of VEGF slightly increased the formation of new bone. Columns show mean values, and error bars represent the corresponding standard deviations (n = 8), *P < 0.05.

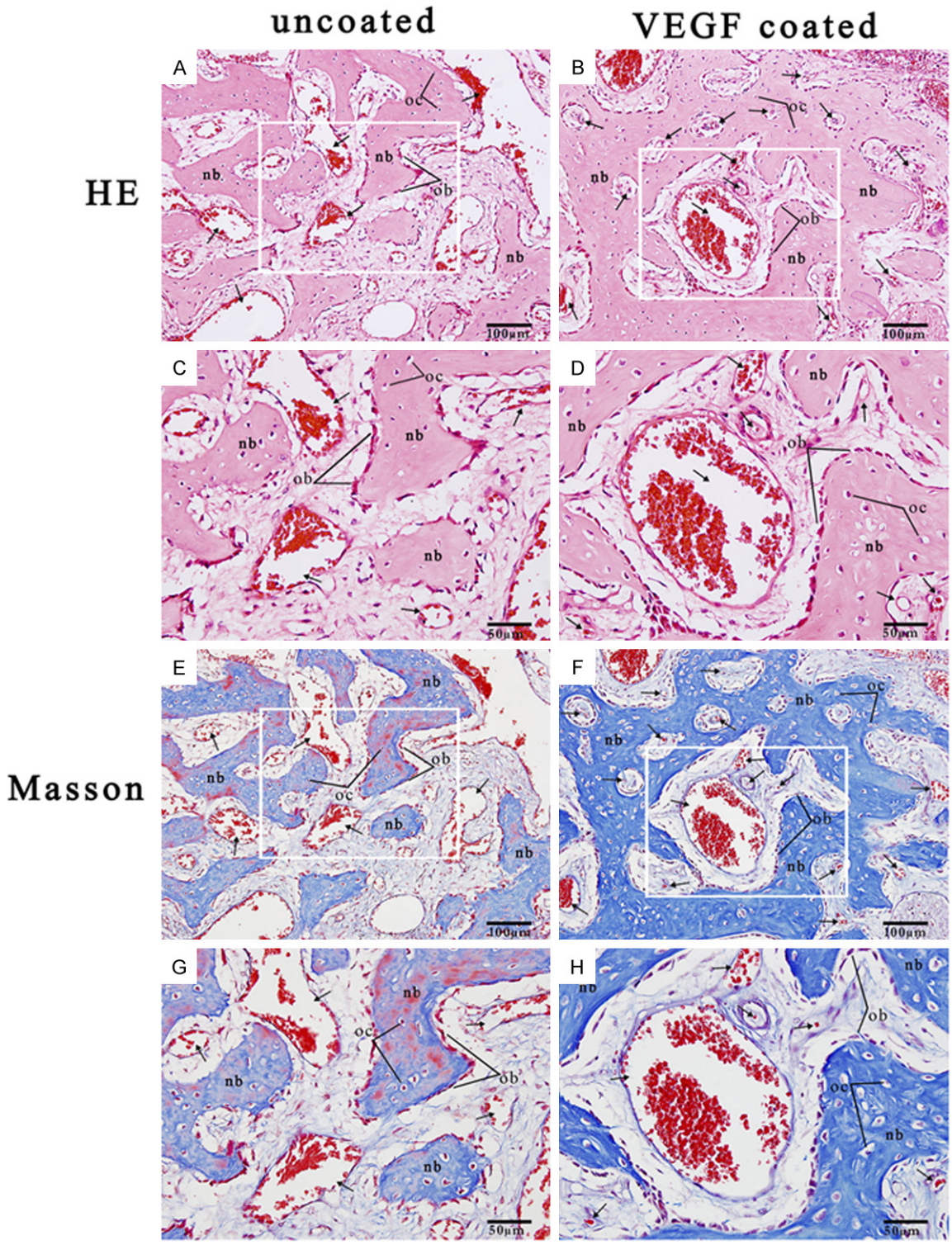

Figure 5. A. HE stained nHA/coral block section (magnification 20 ×). B. HE stained VEGF/nHA/coral block section (magnification 20 ×). C. HE stained nHA/coral block section (magnification 40 ×). D. HE stained VEGF/nHA/coral block section (magnification 40 ×). E. Masson stained nHA/coral block section (magnification 20 ×). F. Masson stained VEGF/nHA/coral block section (magnification 20 ×). G. Masson stained nHA/coral block section (magnification 40 ×). H. Masson stained VEGF/nHA/coral block section (magnification 40 ×). These representative images show the expression of collagen (stained in blue with Masson's stain), newly formed blood vessels (black arrows), new tabular bone (nb), and lines of osteoblasts (ob) and osteocytes (oc) within the scaffolds.

50-mm sections were made. Fluorescent photographs were taken with a laser confocal microscope (Carl Zeiss LSM 510 Meta) aided with appropriate filters. Newly formed mineralized bone in the defects could be distinguished from scaffolds by their respective grey values using ZEN 2009 Light Edition software. The percentage of mineralized bone fill (PMBF = newly formed mineralized bone area/total scaffold area) was calculated with Image-Pro Plus software (Media Cybernetics, USA).

Statistical analysis

All results are expressed as the mean standard deviation (SD) with n = 8. Statistical analyses were performed with SPSS 18.0 (SPSS Inc., Chicago, IL). For the comparisons between groups, a *t*-test was used. The a error was set at 0.05.

Results

Surface morphology and elemental composition of the scaffolds

The porous structure of the nHA/coral blocks was examined with SEM (**Figure 3**). The pores were sufficiently interconnected and distributed, with pore sizes varying from 62-164 μm. The diameter of interconnected pores ranged from 107-550 μm. The nHA crystals were evenly distributed across the surface, with diameters ranging from 71-99 nm.

Histological observations

The post-operative healing was generally uneventful in both animals. No complications, such as swellings, infections, and exposure at grafting sites, were found during the whole study.

From the HE stained images (**Figure 5A-D**), considerable amounts of newly formed trabecular bone and vascular channels were observed both on the surface and in the macropores at the periphery of blocks. This was especially true at the interface between host bone and blocks, while new bone could seldom be found in the center of blocks from both groups. A large number of fibroblast-like cells and some small vessels were observed growing towards the center by the interconnected paths between the macropores. Moreover, some osteoblasts around the macropores of the nHA/coral scaffolds were also observed, which is evidence for the formation of neonatal bone.

Histomorphometric analysis revealed that the percentage of new bone fill (PBF) was 21.7 ± 3.0% and 27.3 ± 8.1% in the nHA/coral and VEGF/nHA/coral groups, respectively. Although the PBF for the VEGF/nHA/coral group was slightly higher than that of the nHA/coral group, there was no significant increase for the VEGF/nHA/coral blocks ($P > 0.05$) (**Figure 4C**).

From the sections stained with Masson's trichrome (**Figure 5E-H**), the expression of collagen (blue-stained tissue) was greater in the VEGF/nHA/coral samples than in the nHA/coral samples. In both groups, the collagen fibers were connected together to form a tabular matrix that allowed mineralization to occur. In addition, for both groups, lines of active osteoblasts were observed around the tabular bone, and a large number of neovascular channels were found.

Immunohistochemical analysis

Immunohistochemical analysis revealed the formation of new blood vessels as characterized by vWF staining of numerous endothelial cells located in vessel basement membranes (**Figure 6**). The distribution of newly formed blood vessels was clearly uneven. Vascular structures were mainly formed at the periphery of the host bone, with fewer formed in the center. Compared to the nHA/coral samples (105 ± 51.8 vessels/mm^2), the VEGF/nHA/coral samples showed an increase in the neovascular density (146 ± 32.9 vessels/mm^2). There was a significant difference between the two groups' neovascular density within the scaffolds ($P < 0.05$) (**Figure 6C**).

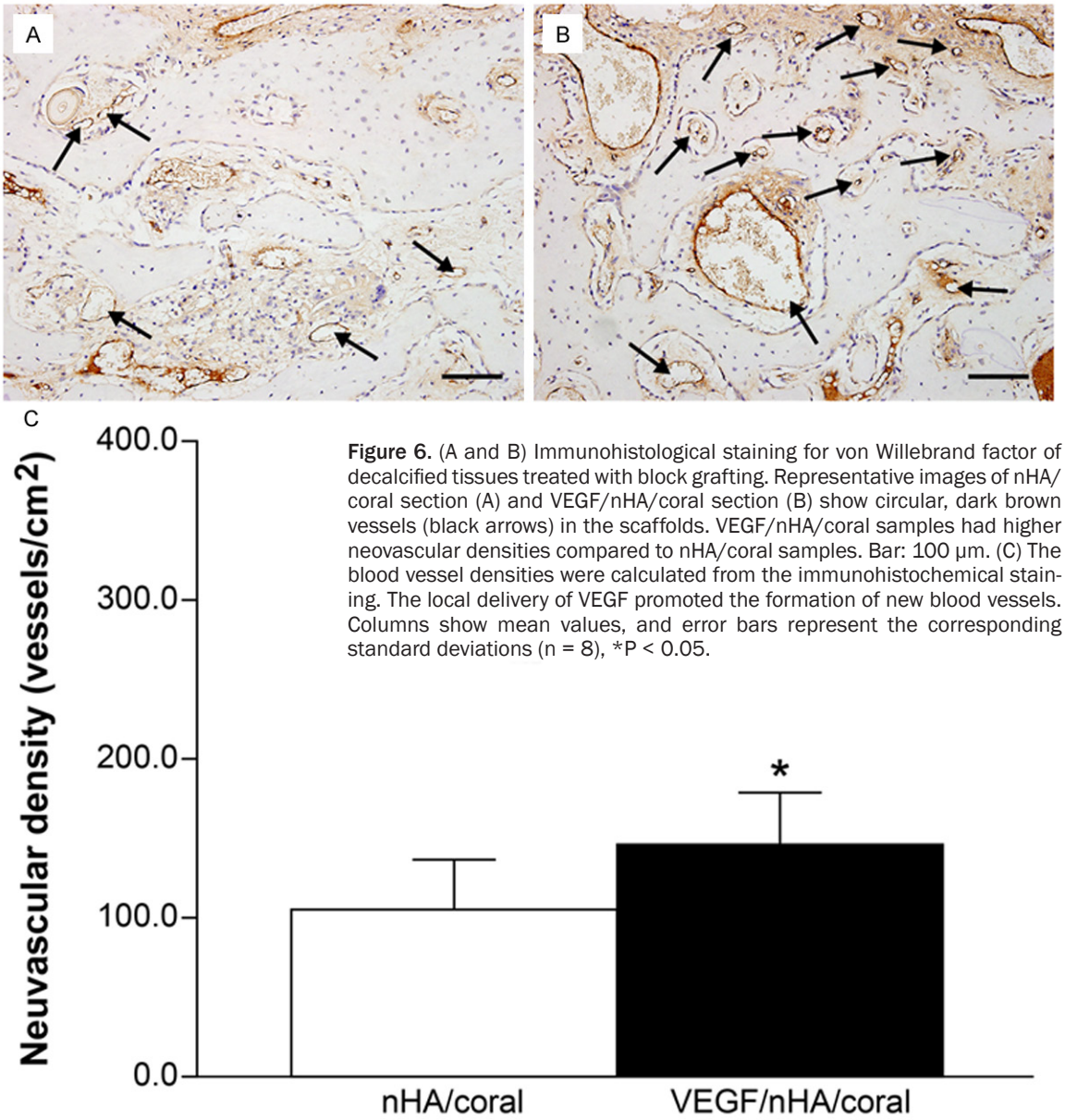

Figure 6. (A and B) Immunohistological staining for von Willebrand factor of decalcified tissues treated with block grafting. Representative images of nHA/coral section (A) and VEGF/nHA/coral section (B) show circular, dark brown vessels (black arrows) in the scaffolds. VEGF/nHA/coral samples had higher neovascular densities compared to nHA/coral samples. Bar: 100 μm. (C) The blood vessel densities were calculated from the immunohistochemical staining. The local delivery of VEGF promoted the formation of new blood vessels. Columns show mean values, and error bars represent the corresponding standard deviations (n = 8), *P < 0.05.

Fluorescence analysis

The ZEN images were analyzed by segmenting the grey values with the imaging software (**Figure 7**). The images show obvious bone regeneration in both groups. The old bone is darker and without labeling, while calcein and tetracycline labeling appear as a diffuse green pattern and thin yellow lines, respectively. The nHA/coral block and the fluorescent, newly mineralized bone can be clearly distinguished.

In both groups, it was observed that new mineralized bone tissue grew on the surface of the blocks, as well as into the macropores at the periphery, but comparatively less was found in the center. In some samples, bone formation was observed even in the interconnected paths without contact with the scaffolds. The shape of the macroporous blocks was maintained; there was no destruction or dissolution of the scaffold surface. Both green and yellow fluorescent lines were found in VEGF/nHA/coral samples, especially at the periphery of the host bone, while yellow lines were seldom found in nHA/coral samples.

Histomorphometrical analysis revealed that the PMBF was 0.79 ± 0.22% for the nHA/coral

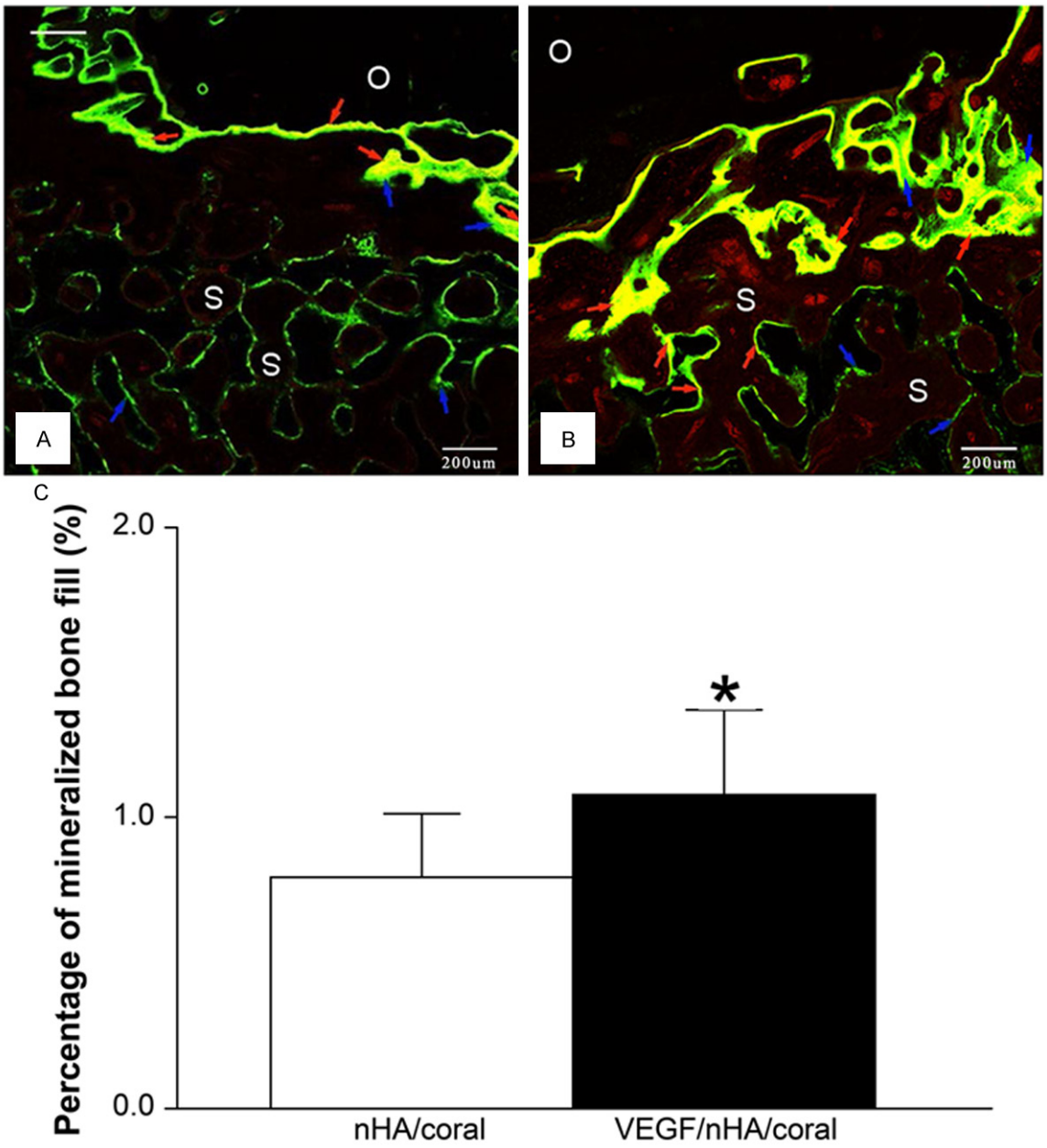

Figure 7. Fluorescence microscopy images of calcified sections show tetracycline- and calcein-stained bone 3 weeks after the implantation of nHA/coral blocks (A) and VEGF/nHA/coral blocks (B). Green lines (blue arrows) that represent the new bone marked by calcein were easily found at the surface of the blocks and inside the scaffold pores in both groups. On the other hand, the yellow lines (red arrows) that represent the new bone labeled with tetracycline were found mainly at the interface between blocks and host bone, and seldom in bone within the macropores. This was especially true for the nHA/coral samples. O: old bone, S: scaffold. (C) The grey values were assigned to different colors and the percentage of mineralized bone fill (PMBF = newly formed mineralized bone area/total scaffold area) was calculated. VEGF/nHA/coral samples showed higher PMBF values compared to nHA/coral samples. Columns show mean values, and error bars represent the corresponding standard deviations (n = 8), *P < 0.05.

group and 1.08 ± 0.29% for the VEGF/nHA/coral group. As shown, there was a significant difference between the PMBF of the two groups, with local delivery of $rhVEGF_{165}$ resulting in increased mineralized bone formation ($P < 0.05$). In addition, compared to nHA/coral samples, more tetracycline-labeled yellow lines were observed in VEGF/nHA/coral samples, which were mainly distributed at the periphery of the host bone.

Discussion

Currently, block grafting materials cannot be widely used in clinics, because of their inability to provide sufficient blood supply and uneven distribution of regenerated bone in the implantation area. Angiogenesis within engineered tissue substitutes is essential in ensuring the proper transportation of nutrients, oxygen, and waste [24]. Previous studies have demonstrated that if a defect reaches a critical size, insufficient nutrition and oxygen transportation is likely to occur, with the oxygen concentration at the center of a large block decreasing [25-27]. Moreover, the diffusion gradients of oxygen and nutrients may influence the cellular proliferation and differentiation within block grafts and, consequently, influence bone formation. In our study, the uneven distribution of newly formed bone and blood vessels was also observed by histological and immunohistochemical analysis. In both groups, newly formed bone and blood vessels could be easily found at the four edges of the scaffolds, whereas they were seldom observed in the center. However, the local delivery of $rhVEGF_{165}$ led to the regeneration of more blood vessels and calcified bone. These results may be attributed to both insufficient blood supply and the different environmental conditions at the periphery and core of the scaffolds. In our defect model, the buccal bone plate was absorbed, with only about 1 or 2 mm of cortical bone maintained. Therefore, the local blood supply was comparatively poor. In addition, the blood vessels and nerves at the bottom of the defects were damaged during the creation of the defects, which led to reduced blood supply in the local area. Moreover, periosteal-releasing incisions during the non-tension suture process may have also destroyed the blood supply in the local area. Hence, the uneven distribution and the above results of the local delivery of VEGF demonstrate that sufficient blood supply plays a crucial role in bone tissue engineering and that the pre-vascularization of block scaffolds is necessary for block grafting.

An ideal scaffold should have an optimal porous structure to allow osteoblasts to grow into the inner parts of the scaffold and to support the vascularization of the ingrown tissue. The pore size of the scaffold is crucial to bone tissue engineering applications. The pores may act as passageways for the transportation of cells and nutrition [28-30]. The larger the pore size, the higher the amount of nutrients and oxygen that can be transported to the inner part of the scaffolds [28]. Scaffolds with comparatively large pores may have more surface area, which can be advantageous for full contact between the graft and body fluid and for the adhesion and proliferation of cells [30-32]. However, if the pores are too large, the mechanical strength may be reduced, which can also affect new bone formation [31]. In addition, good interconnectivity of pores is an important factor for scaffolds. It may increase the surface area as well as enhance the porosity, which are beneficial to the growth of blood vessels, migration of cells, and bone formation [33, 34]. In our study, we used synthetic porous blocks composed of nano-hydroxyapatite and coralline for the grafting material. As shown in the SEM images (**Figure 3**), the nHA/coral blocks have highly interconnected pores with diameters of 107-550 μm, which may permit cellular infiltration of the scaffold. Additionally, in our histological observations, a large number of endothelial cells and active osteoblast cells grew from the edges into the inner part of the scaffold when pre-vascularization was not performed. Moreover, the bone matrix enveloped the surfaces of the macropores via the interconnected paths, as seen in the sections stained with Masson's trichrome. These results indicate that nHA/coral blocks have optimal pore size and interconnectivity of pores.

Fluorescent labeling is a well-established technique for monitoring new bone formation. Fluorochromes are calcium-binding substances that bond with active mineralized bone, thereby labeling the newly formed bone [35-37]. The application of bone markers at different times can record the details of bone formation and remodeling throughout the different stages of bone healing [36]. Calcein and tetracycline fluorochromes emit different colors and provide sequential information when applied at different times [38]. Therefore, in our study, newly calcified bone labeled with tetracycline (yellow lines) revealed the progression of bone regeneration eight days after implantation. Similarly, newly calcified bone marked with calcein revealed the extent of bone formation eighteen days after implantation. For the nHA/coral samples, newly formed bone was mainly

found at the periphery of the scaffolds after 8 days, with none found in the center, while small amounts of newly formed, mineralized bone was observed in the center of the scaffolds for the VEGF/nHA/coral samples. However, after 18 days, newly calcified bone labeled with the two fluorochromes was found within the inner part of the scaffolds for both groups. On the whole, the majority of fluorescent zones were found near the host bone at the borders of the defect, with relatively less found at the center or at a distance from the host bone. Additionally, the evaluation of the ZEN images in the present study revealed that the PMBF of the VEGF/nHA/coral group was significantly greater than that of the nHA/coral group. Interestingly, it appears that the local delivery of VEGF may not lead to uniform improvements in PMBF, PBF, and neovascular density. Significant differences were found in the formation of mineralized bone and blood vessels, whereas there was no statistical difference in bone generation. These results were in accordance with the outcome of a previous study that demonstrated that bioactive glass combined with VEGF can participate in bone healing through indirect processes [22]. These indirect processes enhanced angiogenesis, bone maturation, osteoprogenitor differentiation, and bone formation. From our fluorescent and histomorphometrical analysis, we believe that the local delivery of VEGF using biocoated nHA/coral blocks can improve bone regeneration by accelerating the mineralization process and improving vascularization at the early stages of bone healing.

For the local delivery of growth factors, many aspects may play a crucial role. These include the dose of growth factors, method of coating, release systems, and combination of growth factors delivered [38-41]. A previous study demonstrated that the combined delivery of different doses of VEGF and bone morphogenetic protein-2 (BMP-2) can lead to different effects on bone regeneration [42]. An in vivo, dose-dependent decrease in the PBF was observed for BMP-2, and the subsequent addition of VEGF did not counteract this decrease in the PBF. They also found that the simultaneous release of BMP-2 and VEGF did not increase bone formation over BMP-2 alone after 12 weeks. In a study by Kempen et al., a composite scaffold was created that consisted of poly (lactic-co-glycolic acid) microspheres loaded with BMP-2 embedded in a polypropylene scaffold surrounded by a gelatin hydrogel loaded with VEGF [13]. This in vivo study demonstrated that the local sequential delivery of VEGF and BMP-2 can enhance BMP-2-induced bone formation.

Bone formation is the result of a cascade of events beginning with angiogenesis [43]. Pre-vascularization is crucial for improving the efficacy of block grafting [41, 44-46]. Among the various approaches to scaffold pre-vascularization, the local delivery of angiogenic growth factors is considered one of the most common and practical methods in bone tissue engineering [47, 48]. However, it has disadvantages in that the effect of different doses of single or combined growth factors and the growth factor releasing system are complicated; these issues have not been resolved [13, 42, 49]. For future works, we will attempt to develop a multi-layer composite releasing system with nHA/coral block and other biodegradable carriers and to optimize doses and the sequential delivery of possible cytokine combinations.

Conclusion

This study developed an optimal method for the pre-vascularization of nHA/coral blocks used to graft critical-sized alveolar defects by coating the blocks with $rhVEGF_{165}$. Our findings suggest that the ideal porous structure and nano-sized HA crystals of the nHA/coral blocks play a crucial role in the migration and proliferation of cells, as well as the ingrowth of new bone and blood vessels. Moreover, our results indicate that after being coated with $rhVEGF_{165}$, nHA/coral blocks have an improved early healing response when compared to uncoated nHA/coral blocks by promoting capillary invasion and the formation of new blood vessels and mineralized bone in scaffolds. Therefore, the pre-vascularization of nHA/coral block grafts with VEGF is a promising approach for enhancing vascularized bone regeneration in orthopedic and implant surgery.

Acknowledgements

The authors are especially grateful to Mr Xiaobin Zhu and Mr Shitong Xu (Guangdong Provincial Stomatological Hospital, Southern Medical University, Guangzhou, China) for their support and technical guidance on the graft surgery.

Disclosure of conflict of interest

None.

Address correspondence to: Lei Zhou, Department of Oral Implantology, Guangdong Provincial Stomatological Hospital, Southern Medical University, Guangzhou 510280, China. Tel: +86-20-8423 3801; Fax: +86-20-8443 3177; E-mail: zho668@263.net

References

[1] Polimeni G, Susin C, Wikesjo UM. Regenerative potential and healing dynamics of the periodontium: A critical-size supra-alveolar periodontal defect study. J Clin Periodontol 2009; 36: 258-264.

[2] Lee J, Tran Q, Seeba G, Wikesjo UM, Susin C. The critical-size supraalveolar peri-implant defect model: reproducibility in histometric data acquisition of alveolar bone formation and osseointegration. J Clin Periodontol 2009; 36: 1067-1074.

[3] Xu L, Lv K, Zhang W, Zhang X, Jiang X, Zhang F. The healing of critical-size calvarial bone defects in rat with rhPDGF-BB, BMSCs, and beta-TCP scaffolds. J Mater Sci Mater Med 2012; 23: 1073-1084.

[4] Rentsch C, Rentsch B, Breier A, Spekl K, Jung R, Manthey S, Scharnweber D, Zwipp H, Biewener A. Long-bone critical-size defects treated with tissue-engineered polycaprolactone-co-lactide scaffolds: a pilot study on rats. J Biomed Mater Res A 2010; 95: 964-972.

[5] Mokbel N, Bou SC, Matni G, Naaman N. Healing patterns of critical size bony defects in rat following bone graft. Oral Maxillofac Surg 2008; 12: 73-78.

[6] Yazdi FK, Mostaghni E, Moghadam SA, Faghihi S, Monabati A, Amid R. A comparison of the healing capabilities of various grafting materials in critical-size defects in guinea pig calvaria. Int J Oral Maxillofac Implants 2013; 28: 1370-1376.

[7] Koo KT, Polimeni G, Qahash M, Kim CK, Wikesjo UM. Periodontal repair in dogs: guided tissue regeneration enhances bone formation in sites implanted with a coral-derived calcium carbonate biomaterial. J Clin Periodontol 2005; 32: 104-110.

[8] Devecioglu D, Tozum TF, Sengun D, Nohutcu RM. Biomaterials in periodontal regenerative surgery: effects of cryopreserved bone, commercially available coral, demineralized freeze-dried dentin, and cementum on periodontal ligament fibroblasts and osteoblasts. J Biomater Appl 2004; 19: 107-120.

[9] Yilmaz S, Kuru B. A regenerative approach to the treatment of severe osseous defects: Report of an early onset periodontitis case. Periodontal Clin Investig 1996; 18: 13-16.

[10] Wikesjo UM, Lim WH, Razi SS, Sigurdsson TJ, Lee MB, Tatakis DN, Hardwick WR. Periodontal repair in dogs: a bioabsorbable calcium carbonate coral implant enhances space provision for alveolar bone regeneration in conjunction with guided tissue regeneration. J Periodontol 2003; 74: 957-964.

[11] de Macedo NL, de Macedo LG, Matuda FS, Ouchi SM, Monteiro AS, Carvalho YR. Guided bone regeneration with subperiosteal implants of PTFE and hydroxyapatite physical barriers in rats. Braz Dent J 2003; 14: 119-124.

[12] Boeck-Neto RJ, Artese L, Piattelli A, Shibli JA, Perrotti V, Piccirilli M, Marcantonio EJ. VEGF and MVD expression in sinus augmentation with autologous bone and several graft materials. Oral Dis 2009; 15: 148-154.

[13] Kempen DH, Lu L, Heijink A, Hefferan TE, Creemers LB, Maran A, Yaszemski MJ, Dhert WJ. Effect of local sequential VEGF and BMP-2 delivery on ectopic and orthotopic bone regeneration. Biomaterials 2009; 30: 2816-2825.

[14] Hofmann A, Ritz U, Verrier S, Eglin D, Alini M, Fuchs S, Kirkpatrick CJ, Rommens PM. The effect of human osteoblasts on proliferation and neo-vessel formation of human umbilical vein endothelial cells in a long-term 3D co-culture on polyurethane scaffolds. Biomaterials 2008; 29: 4217-4226.

[15] Ramazanoglu M, Lutz R, Rusche P, Trabzon L, Kose GT, Prechtl C, Schlegel KA. Bone response to biomimetic implants delivering BMP-2 and VEGF: an immunohistochemical study. J Craniomaxillofac Surg 2013; 41: 826-835.

[16] Yang P, Wang C, Shi Z, Huang X, Dang X, Li X, Lin SF, Wang K. RhVEGF 165 delivered in a porous beta-tricalcium phosphate scaffold accelerates bridging of critical-sized defects in rabbit radii. J Biomed Mater Res A 2010; 92: 626-640.

[17] Lode A, Wolf-Brandstetter C, Reinstorf A, Bernhardt A, Konig U, Pompe W, Gelinsky M. Calcium phosphate bone cements, functionalized with VEgf: release kinetics and biological activity. J Biomed Mater Res A 2007; 81: 474-483.

[18] Engsig MT, Chen QJ, Vu TH, Pedersen AC, Therkidsen B, Lund LR, Henriksen K, Lenhard T, Foged NT, Werb Z, Delaisse JM. Matrix metalloproteinase 9 and vascular endothelial growth factor are essential for osteoclast recruitment into developing long bones. J Cell Biol 2000; 151: 879-889.

[19] Mayr-Wohlfart U, Waltenberger J, Hausser H, Kessler S, Gunther KP, Dehio C, Puhl W, Brenner RE. Vascular endothelial growth factor stimulates chemotactic migration of primary human osteoblasts. Bone 2002; 30: 472-477.

[20] Schwarz F, Ferrari D, Balic E, Buser D, Becker J, Sager M. Lateral ridge augmentation using equine- and bovine-derived cancellous bone blocks: a feasibility study in dogs. Clin Oral Implants Res 2010; 21: 904-912.
[21] Schwarz F, Rothamel D, Herten M, Ferrari D, Sager M, Becker J. Lateral ridge augmentation using particulated or block bone substitutes biocoated with rhGDF-5 and rhBMP-2: an immunohistochemical study in dogs. Clin Oral Implants Res 2008; 19: 642-652.
[22] Leach JK, Kaigler D, Wang Z, Krebsbach PH, Mooney DJ. Coating of VEGF-releasing scaffolds with bioactive glass for angiogenesis and bone regeneration. Biomaterials 2006; 27: 3249-3255.
[23] Xiao C, Zhou H, Liu G, Zhang P, Fu Y, Gu P, Hou H, Tang T, Fan X. Bone marrow stromal cells with a combined expression of BMP-2 and VEGF-165 enhanced bone regeneration. Biomed Mater 2011; 6: 15013.
[24] Jonitz A, Lochner K, Lindner T, Hansmann D, Marrot A, Bader R. Oxygen consumption, acidification and migration capacity of human primary osteoblasts within a three-dimensional tantalum scaffold. J Mater Sci Mater Med 2011; 22: 2089-2095.
[25] Volkmer E, Drosse I, Otto S, Stangelmayer A, Stengele M, Kallukalam BC, Mutschler W, Schieker M. Hypoxia in static and dynamic 3D culture systems for tissue engineering of bone. Tissue Eng Part A 2008; 14: 1331-1340.
[26] Malda J, Rouwkema J, Martens DE, Le Comte EP, Kooy FK, Tramper J, van Blitterswijk CA, Riesle J. Oxygen gradients in tissue-engineered PEGT/PBT cartilaginous constructs: Measurement and modeling. Biotechnol Bioeng 2004; 86: 9-18.
[27] Malda J, Klein TJ, Upton Z. The roles of hypoxia in the in vitro engineering of tissues. Tissue Eng 2007; 13: 2153-2162.
[28] Cyster LA, Grant DM, Howdle SM, Rose FR, Irvine DJ, Freeman D, Scotchford CA, Shakesheff KM. The influence of dispersant concentration on the pore morphology of hydroxyapatite ceramics for bone tissue engineering. Biomaterials 2005; 26: 697-702.
[29] Karageorgiou V, Kaplan D. Porosity of 3D biomaterial scaffolds and osteogenesis. Biomaterials 2005; 26: 5474-5491.
[30] Moreau JL, Xu HH. Mesenchymal stem cell proliferation and differentiation on an injectable calcium phosphate-chitosan composite scaffold. Biomaterials 2009; 30: 2675-2682.
[31] Grynpas MD, Pilliar RM, Kandel RA, Renlund R, Filiaggi M, Dumitriu M. Porous calcium polyphosphate scaffolds for bone substitute applications in vivo studies. Biomaterials 2002; 23: 2063-2070.
[32] Klenke FM, Liu Y, Yuan H, Hunziker EB, Siebenrock KA, Hofstetter W. Impact of pore size on the vascularization and osseointegration of ceramic bone substitutes in vivo. J Biomed Mater Res A 2008; 85: 777-786.
[33] Roy TD, Simon JL, Ricci JL, Rekow ED, Thompson VP, Parsons JR. Performance of degradable composite bone repair products made via three-dimensional fabrication techniques. J Biomed Mater Res A 2003; 66: 283-291.
[34] Kruyt MC, de Bruijn JD, Wilson CE, Oner FC, van Blitterswijk CA, Verbout AJ, Dhert WJ. Viable osteogenic cells are obligatory for tissue-engineered ectopic bone formation in goats. Tissue Eng 2003; 9: 327-336.
[35] Sanchez AR, Sheridan PJ, Eckert SE, Weaver AL. Influence of platelet-rich plasma added to xenogeneic bone grafts in periimplant defects: a vital fluorescence study in dogs. Clin Implant Dent Relat Res 2005; 7: 61-69.
[36] Kuzyk PR, Schemitsch EH, Davies JE. A biodegradable scaffold for the treatment of a diaphyseal bone defect of the tibia. J Orthop Res 2010; 28: 474-480.
[37] Lai CH, Zhou L, Wang ZL, Lu HB, Gao Y. Use of a collagen membrane loaded with recombinant human bone morphogenetic protein-2 with collagen-binding domain for vertical guided bone regeneration. J Periodontol 2013; 84: 950-957.
[38] Ikeda J, Zhao C, Chen Q, Thoreson AR, An KN, Amadio PC. Compressive properties of cd-HA-gelatin modified intrasynovial tendon allograft in canine model in vivo. J Biomech 2011; 44: 1793-1796.
[39] Akman AC, Tigli RS, Gumusderelioglu M, Nohutcu RM. BFGF-loaded HA-chitosan: A promising scaffold for periodontal tissue engineering. J Biomed Mater Res A 2010; 92: 953-962.
[40] Roldan JC, Detsch R, Schaefer S, Chang E, Kelantan M, Waiss W, Reichert TE, Gurtner GC, Deisinger U. Bone formation and degradation of a highly porous biphasic calcium phosphate ceramic in presence of BMP-7, VEGF and mesenchymal stem cells in an ectopic mouse model. J Craniomaxillofac Surg 2010; 38: 423-430.
[41] Sun X, Kang Y, Bao J, Zhang Y, Yang Y, Zhou X. Modeling vascularized bone regeneration within a porous biodegradable CaP scaffold loaded with growth factors. Biomaterials 2013; 34: 4971-4981.
[42] Young S, Patel ZS, Kretlow JD, Murphy MB, Mountziaris PM, Baggett LS, Ueda H, Tabata Y, Jansen JA, Wong M, Mikos AG. Dose effect of dual delivery of vascular endothelial growth factor and bone morphogenetic protein-2 on bone regeneration in a rat critical-size defect model. Tissue Eng Part A 2009; 15: 2347-2362.

[43] Sojo K, Sawaki Y, Hattori H, Mizutani H, Ueda M. Immunohistochemical study of vascular endothelial growth factor (VEGF) and bone morphogenetic protein-2, -4 (BMP-2, -4) on lengthened rat femurs. J Craniomaxillofac Surg 2005; 33: 238-245.

[44] Kasten P, Beverungen M, Lorenz H, Wieland J, Fehr M, Geiger F. Comparison of platelet-rich plasma and VEGF-transfected mesenchymal stem cells on vascularization and bone formation in a critical-size bone defect. Cells Tissues Organs 2012; 196: 523-533.

[45] Poh CK, Ng S, Lim TY, Tan HC, Loo J, Wang W. In vitro characterizations of mesoporous hydroxyapatite as a controlled release delivery device for VEGF in orthopedic applications. J Biomed Mater Res A 2012; 100: 3143-3150.

[46] Street J, Bao M, DeGuzman L, Bunting S, Peale FJ, Ferrara N, Steinmetz H, Hoeffel J, Cleland JL, Daugherty A, van Bruggen N, Redmond HP, Carano RA, Filvaroff EH. Vascular endothelial growth factor stimulates bone repair by promoting angiogenesis and bone turnover. Proc Natl Acad Sci U S A 2002; 99: 9656-9661.

[47] Huang YC, Kaigler D, Rice KG, Krebsbach PH, Mooney DJ. Combined angiogenic and osteogenic factor delivery enhances bone marrow stromal cell-driven bone regeneration. J Bone Miner Res 2005; 20: 848-857.

[48] Hernandez A, Reyes R, Sanchez E, Rodriguez-Evora M, Delgado A, Evora C. In vivo osteogenic response to different ratios of BMP-2 and VEGF released from a biodegradable porous system. J Biomed Mater Res A 2012; 100: 2382-2391.

[49] Geuze RE, Theyse LF, Kempen DH, Hazewinkel HA, Kraak HY, Oner FC, Dhert WJ, Alblas J. A differential effect of bone morphogenetic protein-2 and vascular endothelial growth factor release timing on osteogenesis at ectopic and orthotopic sites in a large-animal model. Tissue Eng Part A 2012; 18: 2052-2062.